[55

A. DI GERLANDO, R. PERINI, I. VISTOLI

# MODELLING AND DESIGN ASPECTS OF INVERTER FED SOLID ROTOR SUBMERSIBLE INDUCTION MOTORS FOR PUMPING DRIVES

Proceedings of the ICEM'98
International Conference on Electrical Machines
Vol. 3/3

September 2-4, 1998
Istanbul, Turkey

# ICEM *98* PROCEEDINGS

## Volume III

## International Conference
## on
## Electrical Machines

2 - 4 September, 1998

Istanbul, TURKEY

Organised by:

Middle East Technical University

Istanbul Technical University

# MODELLING AND DESIGN ASPECTS OF INVERTER FED SOLID ROTOR SUBMERSIBLE INDUCTION MOTORS FOR PUMPING DRIVES


**A. Di Gerlando** **R. Perini** **I. Vistoli**

Dipartimento di Elettrotecnica - Politecnico di Milano
Piazza Leonardo da Vinci, 32 - 20133 Milano, Italy



## Abstract

The perspectives of employment of submersible induction motors with solid iron rotor in pumping drives for raising water from deep wells are analysed, considering the inverter supply.

Starting from an equivalent circuit valid for solid rotors, possibly equipped with a conductive coating, the influence of various design and operation motor parameters is investigated, by a comparative analysis among the solutions with solid rotor and cage rotor, in case of supply frequency higher than the mains frequency.


## 1. Introduction

The use of adjustable speed drives is going to be progressively extended to a lot of application sectors, thanks to the increasing availability of reliable and low cost converters, to the easier regulation of the process, to the increase of the energy efficiency of the plants. For example, in the sector of liquid pumping, where the induction motors are widely employed, it is well known that the flow regulation by means of the frequency variation represents a very advantageous solution, compared with the adjustment using shutters, inherently energy wasting, commonly adopted in the past.

Explicit reference is made to the so-called submersible motor, employed for raising the water from underground wells: it is a motor class with special features, whose sizing is usually quite different from that of the standard motors, mainly because of high values of the length/diameter ratio, necessary for limiting the well diameter.

Indeed, the opportunity to be de-coupled by the mains frequency introduces some degrees of freedom, not only in the drive control strategy, but also in the design of each plant component, in particular as regards the motor-pump system.

The most important design choice is the maximum rotational speed; an increase of it, compared with the value obtainable by the mains supply, is surely convenient [7], because:

- being equal the total head and flow of the plant, the size of the pump (to be coupled with the motor supplied at an increased frequency) is significantly lower than that of the needed pump in case of mains supply;
- being equal the core geometry, the output of the motor supplied at an increased frequency is higher compared with that obtainable at mains frequency.

As regards the pump, there are important advantages concerning cost, size, reduction of the shaft length, increase of the lowest critical speeds.

Conversely, as regards the motor, the advantages are partially reduced by a concurrent increase of the losses with the frequency, in particular the mechanical losses, that in these machines are significantly higher than those in the standard induction motors, for the following reasons:

- inside, the machine is full of water (with the double function of cooling fluid and of support for the hydrodynamic bearings);
- the rotor peripheral speed and the significant extension of the surfaces in relative motion produce an important friction loss within the water in the gap, roughly proportional to the third power of the rotational speed and to the fourth power of the rotor diameter [7];
- while the rotor is a roughly smoothed cylinder, the stator surface is not regular, due to the slots, with significant development of turbulence, and then of losses.

The contrasting exigency of a speed increase and of a loss limitation suggests the reduction of the rotor diameter as a possible, straight action; on the other hand, this modification is discouraged, for the following reasons:

- the reduction of the rotor diameter (being equal the electric and magnetic utilisations) implies a reduction of the electromagnetic torque too;
- the cage rotor is not suited to this diameter reduction, considering the needed space for the toothed zone (to place the cage) and for the rotor yoke width (particularly in case of two poles machines); moreover, there is a minimum allowable shaft diameter (for needs of stiffness and mechanical stability of the supports).

The paper analyses the opportunity to adopt a solid rotor structure, possibly equipped with a conductive coating, placed upon the rotor surface.

To this aim, a solid rotor induction motor equivalent circuit is introduced and discussed, for the analysis of the steady-state operation: it is a standard circuit as regards the primary and magnetizing impedances, while it shows two rotor branches, representing the active and reactive effects due to the solid iron core and to the possible conductive coating.

On the basis of this circuit, some motor design aspects are investigated, with the aim of a performance optimisation of the motor-pump system, with inverter supply. Finally, the performances of a solid rotor motor are compared with those of a corresponding cage motor.

## 2. The model of the solid rotor induction motor

The modelling of the solid iron rotors have been initiated a few decades ago and it has been significantly developed, both in terms of analysis methods and as regards the theoretical and experimental results.

Among the theoretical studies, the papers by MacLean [1] and Jamieson [2] must be cited, in which the Maxwell equations have been solved, using the rectangular asymptotic magnetisation curve for the solid rotor:

$$B = +B_S \ \text{for}\ H > 0; \quad B = -B_S \ \text{for}\ H < 0 \quad , \qquad (1)$$

where $B_s$ is the saturation flux density of the material.

These studies have given the basis for the definition of useful models of solid rotor induction motors, with the development of equivalent circuits, validated by tests, both in case of purely ferromagnetic rotor, and in case of solid rotor equipped with conductive coating [3], [4].

Subsequently, the evolution of the computers and of the numerical methods for the electromagnetic field analysis (i.e. the FEM) led to obtain quantitatively more accurate results, thanks to the adoption of more realistic hypotheses (real B(H) curve for the rotor), both for the steady-state and for the transient investigation [5], [6].

Nevertheless, in spite of the limits of the analytical approach and of its circuit implementation, the use of the equivalent circuits allows great advantages, especially for the study of the influence of the various quantities on the fundamental figures of merit of the system. This is particularly useful for the analysis of the design parameter sensitivity, with which the suitability of the solid rotor, to be employed in this application, can be evaluated.

Consequently in the following, after some remarks on the analytical model, the equivalent circuit of the motor is introduced, expliciting its parameters and variables as a function of the constructional and operation quantities.

From the studies performed in [1], [2], [3], [4], the field solution is obtained, as qualitatively illustrated in fig.1; the following hypotheses and remarks are valid:

- the axial length of the rotor is adequately higher than the length $\ell$ of the stator lamination stack; thus, the end effects are considered negligible;
- the stator three-phase winding is considered with quasi-sinusoidal peripheral spatial distribution;
- called $\theta_e$ the peripheral co-ordinate in electrical radians, a sinusoidal spatial flux density distribution $b_g(\theta_e)$ in the gap is assumed, with peak value $B_g$ ; measured $\theta_e$ from the interpolar axis of $b_g(\theta_e)$, we have:

$$b_g(\theta_e) = B_g \cdot \sin(\theta_e)\,; \tag{2}$$

- called z the radial centripetal co-ordinate, measured from the ferromagnetic surface, the rotor (separated from the stator by a mechanical gap of width g and by a possible conductive coating of width d, fixed upon the rotor surface) is magnetised to the saturation limit (at the value $\pm B_s$, typical of the used material) just inside the penetration depth $z_{max} = \delta$;
- within the width $\delta$ there is a line $z_s(\theta_e)$ that divides the zones magnetised at $+B_s$ (sign + valid for the field lines oriented towards negative $\theta_e$ angles) from the zones magnetised at $-B_s$; called $\tau$ the polar pitch (linked with the stator internal diameter D and with the N° of poles p by the well known relation: $\pi \cdot D = p \cdot \tau$), we have:

$$z_s(\theta_e) = \frac{\tau}{2\cdot\pi}\cdot\frac{B_g}{B_s}\cdot\left(1+\cos(\theta_e)\right) \quad \text{for } 0 < \theta_e < \pi$$
$$z_s(\theta_e + n\cdot\pi) = z_s(\theta_e) \quad \text{for each integer n.} \tag{3}$$

The relative motion between the magnetic field in the gap and the rotor (both rotating towards positive $\theta_e$ angles) induces an electric field $k_r$ in the conductive coating and in the rotor zone below $z_s(\theta_e)$; measured $k_r$ positive if entering the draw plane for $0 < \theta_e < \pi$, we have:

$$k_r = -2\cdot\tau\cdot\sin(\theta_e)\cdot B_g\cdot f\cdot x \quad \text{for } -d \le z \le z_s(\theta_e)$$
$$k_r = 0 \quad \text{for } z > z_s(\theta_e)\,; \tag{4}$$

in (4) f is the feeding frequency (in the considered case, the fundamental output frequency of the inverter) and x the slip.

Indicated with $\sigma_c$ and $\sigma_f$ the conductivities of the conductive coating and of the rotor iron respectively, the cross section current densities S [A/m²] are given by:

$$S_c(\theta_e) = \sigma_c\cdot k_r(\theta_e)\ ,\quad S_f(\theta_e) = \sigma_f\cdot k_r(\theta_e)\ , \tag{5}$$

and the linear current densities $\Delta$ [A/m] are expressed by:

$$\Delta_c(\theta_e) = d\cdot S_c(\theta_e)\ ,\quad \Delta_f(\theta_e) = z_s(\theta_e)\cdot S_f(\theta_e)\,. \tag{6}$$

On the basis of (4), $\Delta_c(\theta_e)$ has sinusoidal waveform:

$$\Delta_c(\theta_e) = -\Delta_{cM}\cdot\sin(\theta_e)\ ,\ \text{with} \tag{7}$$

$$\Delta_{cM} = 2\cdot\tau\cdot d\cdot\sigma_c\cdot f\cdot x\cdot B_g\ , \tag{8}$$

while, for (3) and (6), $\Delta_f(\theta_e)$ is distorted: however, just the spatial fundamental harmonic $\Delta_{f1}(\theta_e)$ is assumed representative of the energy conversion:

$$\Delta_{f1}(\theta_e) = -\Delta_{f1M}\cdot\sin(\theta_e + \gamma_f)\ ,\ \text{with} \tag{9}$$

$$\Delta_{f1M} = \frac{\tau^2\cdot\sigma_f/\pi}{B_s\cdot\cos(\gamma_f)}\cdot B_g^2\cdot f\cdot x\ ;\ \gamma_f = \mathrm{atan}\left(\frac{4}{3\cdot\pi}\right) \tag{10}$$

(hence, $\gamma_f \approx 23°$ is a constant displacement angle).

The knowledge of the linear densities $\Delta_{c,f}(\theta_e)$ allows the evaluation of the m.m.f. waves in the gap $m_{c,f}(\theta_e)$:

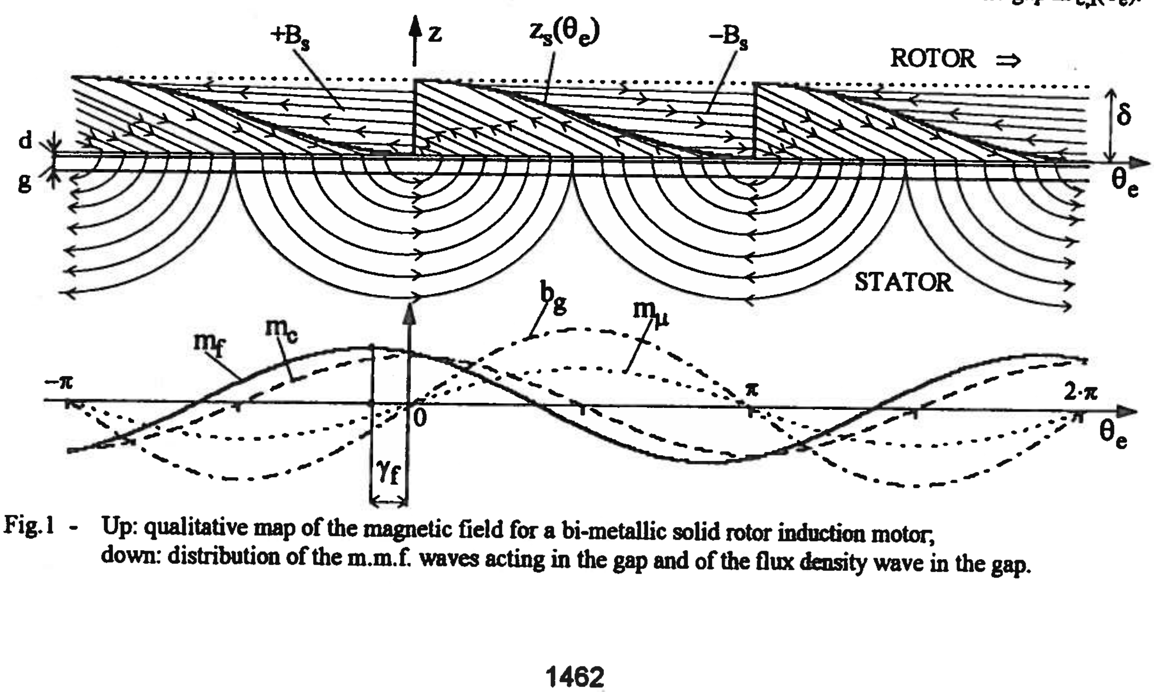


Fig.1 - Up: qualitative map of the magnetic field for a bi-metallic solid rotor induction motor; down: distribution of the m.m.f. waves acting in the gap and of the flux density wave in the gap.

$$m(\theta_e) = \frac{\tau}{\pi} \cdot \int \Delta(\theta_e) \cdot d\theta_e \quad , \tag{11}$$

considering that the integration constant of (11) is defined by the condition that $m(\theta_e)$ has zero average value within two polar pitches; thus, we have:

$$m_c(\theta_e) = M_c \cdot \cos(\theta_e)\,; \quad M_c = \Delta_{cM} \cdot \tau/\pi\,, \tag{12}$$

$$m_f(\theta_e) = M_f \cdot \cos(\theta_e + \gamma_f)\,; \; M_f = \Delta_{f1M} \cdot \tau/\pi\,. \tag{13}$$

Besides the field map, fig.1 shows also the magnetising m.m.f. wave $m_\mu(\theta_e) = M_\mu \cdot \sin(\theta_e)$ (that sustains $b_g(\theta_e)$) and the rotor m.m.f.s $m_c(\theta_e)$ and $m_f(\theta_e)$.

Called $\Phi$ the pole flux, on the basis of (2) we have:

$$\Phi = (2/\pi) \cdot B_g \cdot \tau \cdot \ell \ . \tag{14}$$

For an observer fixed on the stator, the waves of fig.1, in motion rightwards, run in the following sequence: $m_\mu$ (in phase with $b_g$), followed by $m_c$ and finally by $m_f$.

By associating each wave to a space vector with amplitude equal to that of the wave itself and phase corresponding to that of its North magnetic axis ($m_\mu \rightarrow \overline{M}_\mu$ ; $m_c \rightarrow \overline{M}_c$ ; $m_f \rightarrow \overline{M}_f$ ), it follows the vector diagram of fig.2a. This diagram (with vectors rotating in counterclockwise sense) shows also the pole flux vector (with amplitude $\Phi$ and phase coincident with the magnetic axis of $b_g(\theta_e)$) and the m.m.f. vectors $\overline{M}'_c$ and $\overline{M}'_f$ (equal and opposite to the rotor vectors $\overline{M}_c$ and $\overline{M}_f$ ) produced by the reacting stator current components; thus, the total m.m.f. vector $\overline{M}_s$ produced by the stator currents results:

$$\overline{M}_s = \overline{M}_\mu + \overline{M}'_c + \overline{M}'_f \quad . \tag{15}$$

As known, in a three-phase machine the magnetic quantities (m.m.f. M and pole flux $\Phi$, peak values) and the corresponding stator electrical quantities (phase current I and phase flux linkage $\Psi$, RMS values) are linked by the following relations:

$$\Psi = \frac{k_w \cdot U}{2 \cdot \sqrt{2}} \cdot \Phi \quad , \quad I = \frac{\pi \cdot p}{3 \cdot \sqrt{2} \cdot k_w \cdot U} \cdot M \quad , \tag{16}$$

with U N° of stator series connected conductors per phase and $k_w$ winding factor. Thus, it is natural to associate the magnetic diagram of fig.2a to the phasor diagram of fig.2b: in it, besides the current phasors corresponding to the above mentioned m.m.f.s, the phase e.m.f.

$$\overline{E} = j \cdot \omega \cdot \overline{\Psi} \tag{17}$$

is shown ($\omega = 2 \cdot \pi \cdot f$), as well as the voltage drop across stator resistance $R_s$ and leakage reactance $X_s$ and the phase voltage $\overline{V}$; the phasor $\overline{I}'_r = \overline{I}'_c + \overline{I}'_f$ is also shown, i.e. the resultant rotor current referred to one stator phase.

The comparison among the diagrams of fig.2 suggests to extend the validity of (16) also in vector terms.

This analysis allows to deduce the equivalent circuit of the induction motor with solid bi-metallic rotor. To this aim, starting from the definition of the equivalent impedances interested by the rotor currents:

$$\overline{Z}'_c = \overline{E}/\overline{I}'_c \qquad \overline{Z}'_f = \overline{E}/\overline{I}'_f \quad , \tag{18}$$

and on the basis of (12), (13), (14), (16), (17), the circuit of fig.3 is obtained, together with its parameters.

The stator impedance and the magnetising branch are conventional, while the portion equivalent to the rotor is given by two branches in parallel:

– the branch $\overline{Z}'_c = R_c/x$ represents the conductive coating;

– the branch $\overline{Z}'_f = R_f/x + j \cdot X_f$ represents the solid ferromagnetic part of the rotor.

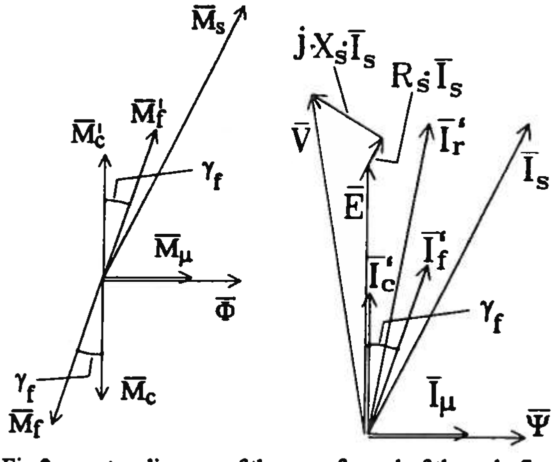


Fig.2a: vector diagram of the m.m.f.s and of the pole flux; fig.2b: phasor diagram of the electrical quantities of each stator phase, corresponding to the diagram of fig.2a.

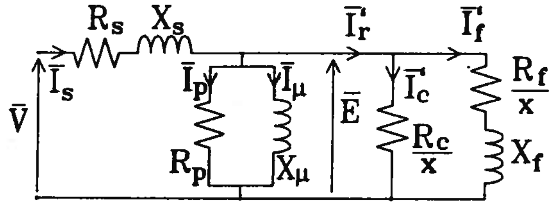


Fig.3 - Equivalent single-phase circuit of a solid rotor induction motor, with conductive coating.

It must be noted that, in addition to the electrical quantities shown in the phasor diagram, the equivalent circuit includes also the loss component $I_p$ of the magnetising current: as usually, this component can be considered separately, in energetic terms.

In the following, the expressions of the parameters $R_s$, $X_s$, $R_p$, $X_\mu$ (known by the theory of the conventional cage induction machine) will not be developed. As regards the rotor parameters, starting from (18), we obtain:

$$R_c = \frac{3 \cdot k_w^2 \cdot U^2 \cdot \ell}{\sigma_c \cdot \tau \cdot p \cdot d} \tag{19}$$

$$R_f = \frac{6 \cdot \pi \cdot k_w^2 \cdot U^2 \cdot \ell}{\sigma_f \cdot p \cdot \tau^2} \cdot \frac{B_s}{B_g} \cdot \cos^2(\gamma_f) \tag{20}$$

$$X_f = \frac{3 \cdot \pi \cdot k_w^2 \cdot U^2 \cdot \ell}{\sigma_f \cdot p \cdot \tau^2 \cdot s} \cdot \frac{B_s}{B_g} \cdot \sin(2 \cdot \gamma_f) \ . \tag{21}$$

The following remarks are valid:

- the model of fig.3 allows also to study the case of a purely ferromagnetic rotor: in fact, the absence of a conductive coating means a coating width d = 0; on the basis of (19), it corresponds to an equivalent infinitive resistance $R_c$, i.e. absence of this branch;
- both the equivalent parameters of the branch representing the ferromagnetic material of the solid rotor ($R_f$, $X_f$) depend on the gap peak flux density, i.e. on the adopted design flux density and on the operating conditions (variations of $B_g$ due to modifications of the voltage drop across the primary impedance $R_s + j \cdot X_s$);
- the equivalent reactance $X_f$ does not depend on the feeding frequency (because the angle $\gamma_f$ does not).

## 3. Energy and design characteristics of the solid rotor induction motor

From the energy point of view, apart from the stator losses (that can be evaluated by means of the classical formulas), it is of interest to calculate the rotor losses: by substituting in the constitutive formulas of these losses

$$P_{pcr} = 3 \cdot R_c \cdot I_c^{\prime 2} \quad , \; P_{pcf} = 3 \cdot R_f \cdot I_f^{\prime 2} \qquad (22)$$

the eq.s (19) and (20) of the resistances and the eq.s of the currents obtainable from the 2nd of (16) (by inserting in it the 2nd of (12) and of (13)), the following expressions of the electrical rotor losses can be obtained:

– rotor losses in the conductive coating $P_{prc}$:

$$P_{prc} = 2 \cdot \pi^3 \cdot \frac{\sigma_c \cdot D^3 \cdot d \cdot \ell}{p^2} \cdot f^2 \cdot B_g^2 \cdot x^2 \; ; \qquad (23)$$

– rotor losses in the solid iron $P_{prf}$ (due to the circulation of the currents induced by the rotating field):

$$P_{prf} = \pi^3 \cdot \frac{\sigma_f \cdot D^4 \cdot \ell}{p^3 \cdot B_s} \cdot f^2 \cdot B_g^3 \cdot x^2 \quad . \qquad (24)$$

Also eq. (23) confirms that, in case of absence of coating (d = 0), the corresponding losses become zero.

It is worth evaluating the ratio among the above mentioned losses ($P_{prc}/P_{prf}$), because it coincides with the ratio of the corresponding powers electromagnetically transferred through the gap and, therefore, with the ratio of the electromagnetic torque contributions ($T_{ec}/T_{ef}$):

$$\frac{P_{prc}}{P_{prf}} = \frac{T_{ec}}{T_{ef}} = 2 \cdot p \cdot \frac{\sigma_c}{\sigma_f} \cdot \frac{d}{D} \cdot \frac{B_s}{B_g} \quad . \qquad (25)$$

The following comments can be made:

– while the single rotor electrical losses depend on the frequency (f) and on the slip (x), i.e. on the operating conditions, their ratio (as like as the ratio of the torque contributions) does not; moreover, (25) shows the dependence on the peak value of the flux density at the gap ($B_g$), that does not change very much during the operation;

– chosen the number of poles (p), the geometry (d, D), the characteristics of the materials ($B_s$, $\sigma_f$, $\sigma_c$), if the operating flux density $B_g$ is weakly variable, also the above mentioned ratio is roughly constant; this allows to design the coating in such a way to produce a desired torque contribution, in addition to that generated by the solid iron rotor; for example, with $p = 2$, $\sigma_c/\sigma_f \approx 15$, $d/D \approx 5 \cdot 10^{-3}$, $B_s/B_g \approx 2.5$, one obtains:
$$T_{ec}/T_{ef} = P_{prc}/P_{prf} \approx 0.75 \, .$$

Moreover, it is important to note that the adoption of a conductive coating implies some negative consequences, of constructional and operational nature:

– this superposition requires a complex manufacturing technology (electrolytic deposition upon the iron rotor cylinder, or forcing of a heated pre-shaped hollow cylinder, with very restricted tolerances);

– being equal the mechanical gap (that cannot be reduced to prevent grazing risks during the operation), the magnetic gap $g_\mu$ increases of a quantity equal to the width d of the coating ($g_\mu = g + d$), with significant increases of the magnetising current $I_\mu$.

The electromagnetic torque $T_e$ can be expressed by means of the power $P_t$ transferred through the gap:

$$T_e = \frac{P_t}{\Omega_0} = \frac{P_{prc} + P_{prf}}{x \cdot \omega/(p/2)} = \frac{p \cdot P_{prf}}{4 \cdot \pi \cdot f \cdot x} \cdot \left(1 + \frac{P_{prc}}{P_{prf}}\right) . \qquad (26)$$

Also (26) is valid in general, because in case of absence of coating, the term within brackets reduces to unity.

By developing (26) on the basis of (24) and (25) one obtains:

$$T_e = \frac{\sigma_f \cdot D^4 \cdot \ell \cdot f \cdot B_g^3 \cdot x}{(2/\pi)^2 \cdot p^2 \cdot B_s} \cdot \left(1 + 2 \cdot p \cdot \frac{\sigma_c}{\sigma_f} \cdot \frac{d}{D} \cdot \frac{B_s}{B_g}\right) . \qquad (27)$$

Eq.(27) suggests the following comments:

– the electromagnetic torque linearly depends on the active length $\ell$, but it is function of the 4th power of the rotor diameter D;

– the torque contribution due to the "iron" is directly proportional to the steel conductivity $\sigma_f$: thus, it would be convenient to employ steel alloys with low resistivity (for example, with a suited copper content);

– in case of adoption of the coating, this contributes to the torque production proportionally to its width d.

The analysis of the cage motor [7] has already shown that an important loss item is given by the mechanical friction losses $P_{pm}$; the corresponding torque, $T_{pm}$, depends on the sizes and on the rotational speed $\Omega$ [rad/s]:

$$T_{pm} = \frac{P_{pm}}{\Omega} = k_{pm} \cdot D^4 \cdot \ell \cdot \Omega^2 \quad , \qquad (28)$$

where $k_{pm}$ is a coefficient depending on the Reynolds number and on the equivalent roughness of the faced stator and rotor surfaced; developing $\Omega$, one obtains:

$$T_{pm} = (4 \cdot \pi/p)^2 \cdot k_{pm} \cdot D^4 \cdot \ell \cdot f^2 \cdot (1-x)^2 \quad . \qquad (29)$$

Eq.(29) suggests that, in order to reduce the hydrodynamic friction torque, the diameter D can be reduced: in fact, it is enough a 15% diameter D reduction to halve the friction losses, being equal the other quantities.

Unfortunately, if one of the other quantities is not modified, the electromagnetic torque decreases with the same rate, as can be deduced by (27): in this case the performances become unacceptable. In fact, dividing (27) by (29), one obtains:

$$\frac{T_e}{T_{pm}} = \frac{1 + 2 \cdot p \cdot \frac{\sigma_c}{\sigma_f} \cdot \frac{d}{D} \cdot \frac{B_s}{B_g}}{64 \cdot (B_s/\sigma_f) \cdot k_{pm}} \cdot \frac{x \cdot B_g^3}{f \cdot (1-x)^2} \quad . \qquad (30)$$

Eq.(30) shows that the most important quantity suited to sustain the ratio $T_e/T_{pm}$ is the peak flux density $B_g$ in the gap: the higher the gap flux density, the more favourable the above defined ratio; of course, the values of $B_g$ to be adopted must be compatible with the constructional, magnetic and power constraints of the machine.

To this aim, considering that the following is valid

$$\Phi = \frac{2}{\pi} \cdot B_g \cdot \tau \cdot \ell = \frac{2}{p} \cdot B_g \cdot D \cdot \ell \quad , \qquad (31)$$

the flux density $B_g$ can be expressed as follows:

$$B_g = \frac{p}{2} \cdot \frac{\Phi}{D \cdot \ell} = \frac{p}{2} \cdot \frac{\Phi_\ell}{D} \quad , \qquad (32)$$

where $\Phi_\ell = \Phi/\ell$ is the pole flux, referred to the active length of the machine.

By elaborating the known relations linking the flux in the gap with the flux in the teeth and in the stator yoke, one obtains the following expressions of the tooth width $b_t$ and of the radial height of the stator yoke $h_y$:

$$b_t = \frac{\pi}{6 \cdot q_s} \cdot \frac{(1+\varepsilon_{\ell t}) \cdot \Phi_\ell}{K_s \cdot B_t} \quad , \; h_y = \frac{1}{2} \cdot \frac{(1+\varepsilon_{\ell y}) \cdot \Phi_\ell}{K_s \cdot B_y} \quad , \tag{33}$$

with $K_s$ lamination stacking factor, $q_s$ number of stator slots/(pole·phase), $B_t$ and $B_y$ flux densities in the teeth and in the stator yoke, $\varepsilon_{\ell t}$ and $\varepsilon_{\ell y}$ raising coefficients taking into account the stator leakage.

The insertion of (32) into (27) leads to:

$$T_e = \frac{\pi^2 \cdot \sigma_f}{32 \cdot B_s} \cdot p \cdot \Phi_\ell^3 \cdot D \cdot \ell \cdot f \cdot x \cdot \left(1 + 4 \cdot \frac{\sigma_c}{\sigma_f} \cdot \frac{B_s \cdot d}{\Phi_\ell}\right) . \tag{34}$$

Eq.s (32), (33), (34) suggest that:

- a possible way to sustain the electromagnetic torque when decreasing the internal diameter D, taking advantage of the reduction of the friction losses, consists in reducing the diameter D maintaining constant the pole flux per active unit length $\Phi_\ell$;
- by this modification, the peak flux density $B_g$ in the gap increases according 1/D; conversely (on the basis of (33)) the condition $\Phi_\ell$ = constant is compatible also with unmodified values of flux densities and widths of the stator core magnetic branches;
- of course, the reduction of the internal diameter D must satisfy the constructional constraints, among which an acceptable slot opening, in order to easily insert the winding: in fact, the reduction of D implies the lengthening of the teeth, whose heads tend to approach each others, with reciprocal interference, due to the curvature effect in the gap;
- moreover, if we suppose to increase the active length $\ell$ proportionally to 1/D, from (34) it follows that the electromagnetic torque remains unmodified: this lengthening is possible because, in case of solid rotor, the electromagnetic active diameter of the rotor is also effective as regards the shaft stiffness (because the rotor coincides with the shaft itself); on the contrary, in case of the cage rotor, the electromagnetic active diameter of the rotor is the lamination diameter, ineffective as regards the shaft stiffness; thus, we can assume that the shaft diameter in case of solid rotor can be greater compared with that of the cage laminated rotor; so, this higher stiff-effective diameter allows the growth of $\ell$, without increasing the risk of occurrence of bending critical speeds within the useful operating range.

As regards the machine electrical losses, we can recognise that:

- on the basis of (23) and (24), the above mentioned dimension and operating variations do not modify the losses in the rotor iron and in the coating, if existing;
- about the stator losses, the invariance of the flux density in the core implies that the specific core losses do not change: however, the actual losses in the stator core increase because both the teeth height and the active length $\ell$ increase;
- the evaluation of the stator winding losses requires a more detailed analysis: in fact, on the one hand, they increase due to the increase of $\ell$, while it is not simple to estimate the effect of the increase of the slot area (favourable) and the effect of the increase of the peak flux density $B_g$ in the gap and of the teeth length (that surely increase the magnetising current).

In order to show the effects of the parameter variations, it is better to express all the quantities in p.u., referred to the corresponding initial reference values and to indicate all the p.u. variables with the same symbol of the actual variable, surmounted by a point.

Considering now to progressively reduce the diameter D at the gap, from the hypothesis:

$$\dot{\Phi}_\ell = 1 \tag{35}$$

with

$$\dot{\ell} = 1/\dot{D} \tag{36}$$

it follows the invariance of the electromagnetic torque $T_e$, of the tooth width $b_t$, of the stator yoke height $h_y$, of the flux density in the tooth $B_t$ and in the stator yoke $B_y$, hence:

$$\dot{T}_e = \dot{b}_t = \dot{h}_y = \dot{B}_t = \dot{B}_y = 1 \; . \tag{37}$$

On the basis of (36), the p.u. friction torque results:

$$\dot{T}_{pm} = \dot{D}^4 \cdot \dot{\ell} = \dot{D}^3 \, . \tag{38}$$

Fig.4 shows the behaviour of (36), (37) and (38), under the condition (35): it is clear a significant reduction of the friction torque when diminishing D, with invariance of the electromagnetic torque.

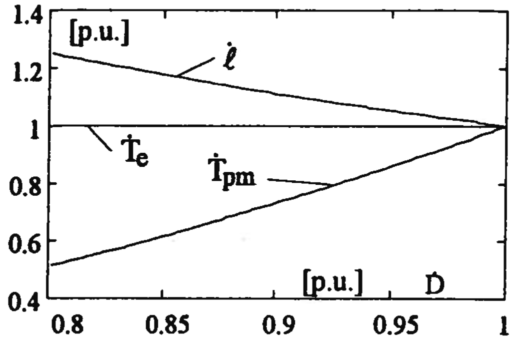


Fig.4 - Stator lamination stack length, electromagnetic and friction torques as a function of the internal diameter, under the conditions (35), (36); values expressed in p.u..

For example, if one supposes to reduce the internal diameter to the value:

$$\dot{D} = 0.85 \, ;$$

the following values of the other quantities result:

$$\dot{\Phi}_\ell = 1 \;\Rightarrow\; \dot{\ell} = \dot{B}_g = 1/\dot{D} \approx 1.18 \; ,$$

$$\dot{T}_{pm} = \dot{D}^4 \cdot \dot{\ell} = \dot{D}^3 \approx 0.61 \, .$$

Thus, a marked reduction of the friction losses can be obtained, allowing a corresponding improvement of the efficiency and of the thermal condition of the machine; in fact, we can assume that, even if reducing the internal diameter D, the external diameter $D_e$ of the machine could remain unmodified; this condition involves that:

- being unmodified the yoke height $h_y$ and the tooth width $b_t$, the reduction of D implies an increase of the available slot section (even if moderate, considered the effect of the teeth convergence, due to the curvature);
- the increase of $\ell$, being equal the external diameter $D_e$, implies the increase of the cooling surface of the frame, with improvement of the heat exchange.

## 4. Performance comparison

In the following, the previous analyses are applied to the sizing of different two-pole solid rotor induction motors: their calculated performances are compared with those of a two-pole motor equipped with a cage rotor (with bars and rings made of copper), really constructed, having the basic data of Table I (see also [7]).

Table I - Rated, operating and constructional data of the submersible induction motor with copper cage, chosen for the comparison with the solid rotor induction motors.

| | |
|---|---|
| Rated voltage and power: $V_n$ [V] - $P_n$ [kW] | 380 - 30 |
| N° of poles - rated frequency: p - $f_n$ [Hz] | 2 - 50 |
| rated efficiency: $\eta_n$ [%] | 86.6 |
| rated power factor: $\cos\varphi_n$ | 0.876 |
| rated slip: $x_n$ [%] | 3.2 |
| rated flux density at the gap: $B_{gn}$ [T] | 0.64 |
| rated stator current density: $S_{sn}$ [A/mm²] | 10.6 |
| stator extern.- intern. diameter: $D_e$ - D [mm] | 186 - 96 |
| number of stator slots/(pole·phase): $q_s$ | 4 |
| stator tooth width: $b_{ts}$ [mm] | 5 |
| stator yoke radial height: $h_{ys}$ [mm] | 19.5 |
| stator lamination stack length: $\ell$ [mm] | 450 |
| stator slot opening: $b_a$ [mm] | 4.7 |
| shaft diameter in the active zone: $D_{sh}$ [mm] | 65 |

The comparative analysis, based on the equivalent circuit of fig.3 and resumed in Table II, has been performed by maintaining constant some common data (see caption of Table II); it is particularly important the invariance of:

- frame external diameter ($D_e$): it is a dimension constrained by the well diameter;
- mechanical gap (g): in case a conducting coating is adopted, the magnetic gap $g_\mu$ results g + d;
- losses that can be dissipated by the frame, per unit length of the lamination stack ($P_{pd}/\ell$): this parameter defines the global conditions of thermal exchange towards the well; the same value of $P_{pd}/\ell$ for different machines means a roughly equal internal thermal state: this condition, when considered in steady state operation, defines the total admissible motor losses;
- rotational speed (N): it allows an homogeneous comparison as regards the items friction losses and power output (the chosen value - N = 4200 rev/min - is that of the maximum output for the machine of Table I [7]);
- slot opening ($b_a$): the adopted value corresponds to the minimum stator diameter, being equal the tooth width (thus, being equal the tooth flux density).

The analysis of the data of Table II (that refers to three internal diameter values and to three length values of the stator lamination stack) suggests the following remarks:

- the friction losses are an important portion of the total losses, especially for the motors 1, 2, 3, having the highest D: thus, a reduction of these losses is essential in order to improve the performances;
- the motor 1, of the cage type, has the same rotor and magnetic structure of that of Table I, apart from the winding adaptation for the supply with increased frequency: there is a significant increase of the power output, accompanied by an important size reduction of the coupled pump [7];
- the motor 2 (equipped with solid rotor, without coating, having the same D and $\ell$ sizes of the cage motor 1) has output power greatly lower than that of the motor 1, with low values of efficiency and power factor, mainly because of its higher rotor losses: this result shows that, without suited modifications, the solid rotor produces discouraging performances;
- the motor 3, corresponding to 2, with the addition of a copper coating (d = 0.5 mm) improves the performances slightly, even if they remain insufficient;
- the motor 4 shows a first significant modification, with the reduction of D (being equal $\Phi_\ell$ and $\ell$) to the minimum value, compatible with unmodified tooth width and slot opening: the invariance of $\Phi_\ell$ when diminishing D implies an increase of $B_g$ (with magnetising current increase, but unmodified core flux density); concerning the performances, the following can be noted: there is a clear reduction of the friction losses, with an improvement compared with the situation of the motor 2 (homogeneous with the motor 4, being without coating too); anyway, the output does not ameliorate compared with that of the motor 3 (both for the absence of the coating and considering that the invariance of $\ell$ does not compensate the reduction of D -on the basis of (34)-);
- the motor 5 shows an improvement compared with the motor 4, thanks to the use of the copper coating (with d = 0.5 mm): the efficiency is higher than before, but the power output is again lower than that of the motor 1;
- the motor 6 (without coating) implements the second important dimensional modification of the machine, i.e. the increase of the active stack length $\ell$ (proportionally to 1/D, compared with the motor 1); this modification implies two favourable consequences: the support of the electromagnetic torque (thanks to (34), (35), (36)) and the increase of the heat that can be dissipated by

Table II - Comparison between induction motors with cage and solid rotor (with and without copper coating):
rotor type classification: ***cr*** = cage rotor; ***sr*** = solid rotor ; ***srcc*** = solid rotor with copper cylinder (d = width).
Common data: poles = 2; speed: N = 4200 rev/min; $\rho_c$= 0.020 μΩ·m; $\rho_f$ = 15·$\rho_c$; $B_s$= 1.7 T; st. ext. Ø: $D_e$= 186 mm; specific losses that can be dissipated: $P_{pd}/\ell$ = 14.8 kW/m; st. slot opening: $b_a$ = 4.7 mm; mechanical gap: g = 1 mm.

| Motor N° | $q_s$ | rotor type | cylind. width d [mm] | int st Ø D [mm] | stack len. $\ell$ [mm] | output power [kW] | friction loss [kW] | st Fe loss [kW] | st Cu loss [kW] | rot Cu loss [kW] | rot Fe loss [kW] | eff. η [%] | pwr. f. cosφ [p.u.] | slip x [%] | st curr. dens. $S_s$ A/mm² | gap flux d. $B_g$ [T] | tot rot loss / $\ell$ [kW/m] |
|---|---|---|---|---|---|---|---|---|---|---|---|---|---|---|---|---|---|
| 1 | 4 | ***cr*** | - | 96 | 450 | 38.9 | 3.32 | 0.80 | 1.59 | 0.95 | - | 85.4 | 0.895 | 2.20 | 9.93 | 0.622 | 9.5 |
| 2 | 4 | ***sr*** | 0 | 96 | 450 | 14.6 | 3.32 | 0.83 | 0.65 | 0 | 1.86 | 68.7 | 0.581 | 4.91 | 6.13 | 0.625 | 11.5 |
| 3 | 4 | ***srcc*** | 0.5 | 96 | 450 | 22.0 | 3.32 | 0.82 | 0.98 | 0.46 | 1.08 | 76.8 | 0.665 | 3.79 | 7.53 | 0.625 | 10.8 |
| 4 | 4 | ***sr*** | 0 | 74 | 450 | 21.1 | 1.17 | 0.96 | 0.82 | 0 | 3.71 | 76.0 | 0.545 | 7.68 | 6.49 | 0.811 | 10.8 |
| 5 | 4 | ***srcc*** | 0.5 | 74 | 450 | 31.3 | 1.17 | 0.94 | 1.27 | 0.98 | 2.31 | 82.5 | 0.635 | 6.16 | 8.07 | 0.811 | 9.9 |
| 6 | 4 | ***sr*** | 0 | 74 | 585 | 27.6 | 1.52 | 1.25 | 1.00 | 0 | 4.87 | 76.1 | 0.547 | 7.72 | 6.51 | 0.811 | 10.9 |
| 7 | 4 | ***srcc*** | 0.5 | 74 | 585 | 41.1 | 1.52 | 1.22 | 1.55 | 1.30 | 3.05 | 82.6 | 0.638 | 6.21 | 8.11 | 0.811 | 10.0 |
| 8 | 3 | ***sr*** | 0 | 65 | 665 | 31.7 | 1.03 | 1.49 | 1.13 | 0 | 6.18 | 76.3 | 0.516 | 8.61 | 6.55 | 0.923 | 10.8 |
| 9 | 3 | ***srcc*** | 0.5 | 65 | 665 | 47.2 | 1.03 | 1.45 | 1.78 | 1.66 | 3.91 | 82.8 | 0.599 | 6.98 | 8.21 | 0.923 | 9.9 |
| 10 | 3 | ***srcc*** | 0.75 | 65 | 665 | 52.7 | 1.03 | 1.44 | 2.11 | 2.05 | 3.21 | 84.3 | 0.610 | 6.36 | 8.94 | 0.923 | 9.5 |

of the allowable losses); there is an improvement compared with the motor 4, even if again not sufficient (also because of the increase of the friction losses, proportional to the increase of $\ell$);

- the motor 7, corresponding to the motor 6, with copper coated rotor (again with d = 0.5 mm), represents the first solution allowing a power output higher than that of the motor 1; also the efficiency is quite acceptable, while the power factor remains low (because of the already mentioned increase of the magnetising current, due both to the increase of $B_g$ and to the higher magnetic voltage drop in the stator teeth, longer than those of the case 1): of course, in case the improvement would be limited to this moderate increase of the power output compared with that of the motor 1, the employment of the solid rotor would be not justified at all;
- the motor 8 shows the effect of the third kind of substantial modification of the design, i.e. the choice of a lower number of slots/(pole·phase) $q_s$: this option allows a further reduction of the internal diameter, accompanied by an increase of $\ell$, on the basis of (35) and (36): the homogeneous case is that of the motor 6, and the comparison with it shows an increase of the power output, thanks to the reduction of the friction losses and to the increase of the power that can be dissipated by the frame; anyway, the power output and the efficiency are again lower than those of the motor 1, due to the absence of the coating;
- the motor 9 corresponds to the previous one, with the rotor equipped with the copper coating (again with d = 0.5 mm): the power output becomes interesting, as like as the efficiency, but the power factor remains low;
- the motor 10 has the same active sizes (D, $\ell$) of the motors 8 and 9, but the width of the coating has been increased of 50% (d = 0.75 mm): the power output is roughly 35% higher than that of the motor 1, with an efficiency slightly lower; it is a solution actually advantageous, that shows the convenience to adopt a solid rotor in this application.

As regards the actual feasibility of a motor like the motor N° 10, the following comments can be added:

- from the mechanical point of view, the reduction of D and the corresponding increase of the active length $\ell$ do not imply particular risks for the bending vibrations: in fact, D = 65 mm coincides with the original shaft diameter of the motor 1 (see Table I): thus, the shaft of the motor 10 has the same stiffness per unit length (as already remarked, the rotor lamination of the motor 1 does not give contributions); moreover, considering that the shaft is much longer than the active length $\ell$, an increase of $\ell$ does not imply a significant stiffness reduction; in conclusion, the 1st bending critical speed remains surely well above N = 4200 rev/min;
- concerning the electrical aspects, the low power factor implies, if not compensated, a current oversizing of the inverter valves: however, it is possible to insert some capacitors as power factor correctors; they contribute also to the filtering of the switching over-voltages generated by the PWM inverter;
- from the thermal point of view (and as a completion of the criterion of the same specific power dissipated by the frame) we can add the following remarks: the temperature rise among active sides and slot water is surely lower in the cases 2, 3,..., 10 than in the case 1 (this temperature rise is mainly due to the stator winding losses, that are lower because the current density $S_s$ is lower); also the total rotor losses divided by the length $\ell$ ((friction + fe rot + cu rot)/$\ell$) are quite similar to those of the motor 1, with quite similar heating of the water in the gap channel.

## 5. Conclusions

In the present paper an analytical approximated model of the solid rotor induction motor has been described, possibly equipped with a conductive coating.

The corresponding equivalent circuit has led to define the dependence of parameters and performances on the main constructional and operating quantities of the machine, allowing the analysis of the effect of several design modifications, especially the reduction of the diameter at the gap and the increase of the active length, being equal the pole flux per active lamination stack length.

Different design solutions have been analysed, with or without conductive coating, considering the variation of the active sizes and of the number of stator slots, quantitatively comparing their performances.

The result of the comparison is that a solid rotor motor represents certainly a quite interesting solution.

Of course, a more accurate evaluation of the actual performances requires the refinement of the electromagnetic analysis, an effective design of the internal hydrodynamic circuit (for the cooling) and a suited thermal model (for the analysis of the temperature distribution, on which the performances depend strictly). These refinements will be the objects of the next research activities.

## References


[1] W. MacLean: "Theory of Strong Electromagnetic Waves in Massive Iron", Journal of Applied Physics, Vol.25, N°10, October 1954, pp.1267-1270.

[2] R. A. Jamieson: "Eddy-current effects in solid, unslotted iron rotors", Proc.IEE, Vol.115, N°6, June 1968, pp.813-820.

[3] R. Manigrasso, I. Vistoli: "Motori a induzione con indotto massiccio", Journal "L'Energia Elettrica", N°12, 1969, pp.875-882 (in Italian).

[4] R. Manigrasso, G. Petrecca: "Motori a induzione con rotore massiccio bimetallico", Journal "L'Energia Elettrica", N°6, 1971, pp.387-395 (in Italian).

[5] B. Brunelli, D. Casadei, U. Reggiani, G. Serra: "Transient and Steady-State Behaviour of Solid Rotor Induction Machines", IEEE Trans. on Mag., Vol.Mag-19, N°6, November 1983, pp.2650-2654.

[6] J. M. Biedinger, S. Poullain, J. P. Yvon: "Optimal Control of the Torque of Solid Iron Rotor Induction Motor", IEEE Trans. on Mag., Vol.28, N°2, March 1992, pp.1585-1588.

[7] A. Di Gerlando, R. Perini, I. Vistoli, G. Bosi: "Design and Operation Improvements of Inverter Fed Adjustable Speed Induction Motors for Pumping Applications", Proceedings ICEM'96, Vigo, Spain, 10-12 September 1996.